Preprints of the 21st IFAC World Congress (Virtual)
Berlin, Germany, July 12-17, 2020

Inversion Based Adaptive Feedforward Control for Multivariable Systems

Shahin Rouhani * **Sandeep Rai** ** **Tsu-Chin Tsao** ***

* *University of California Los Angeles, Los Angeles, CA 90095 USA (e-mail: shahin.rouhani@engineering.ucla.edu).*
** *University of California Los Angeles, Los Angeles, CA 90095 USA (e-mail: sandyrai00@g.ucla.edu)*
*** *University of California Los Angeles, Los Angeles, CA 90095 USA (e-mail: ttsao@seas.ucla.edu)*

Abstract: This paper presents a novel adaptive feedforward control (AFC) method for rejecting sinusoidal disturbances with known frequencies acting on multi-input-multi-output (MIMO) discrete time linear systems based on the H-infinity synthesis. First, the gradient AFC (GAFC) for MIMO systems is reviewed, and the linear time invariant (LTI) equivalent form of the GAFC is approximated for stability analysis. For single-input-single-output (SISO) systems, this paper shows small adaptation gains guarantee the stability of GAFC for any disturbance frequency. Then inspired by the stability of SISO GAFC, the inversion based AFC (IAFC) is proposed for MIMO systems. In this method, the GAFC is compensated by an H-infinity model matching filter, which renders nearly decoupled systems with fixed time delays. The LTI analysis, simulation study and experimental results from an open-loop unstable MIMO Active Magnetic Bearing Spindle (AMBS) are presented to demonstrate the stability and effectiveness of the proposed IAFC in rejecting narrow-band disturbances.

Keywords: adaptive algorithm, multivariable system, optimization, active magnetic bearing, high speed machining

1. INTRODUCTION

Disturbance rejection has been of great interest to researchers in control and signal processing communities. If disturbances are measurable, a feedforward strategy can attenuate their influence. Otherwise, feedback algorithms based on disturbance observers have been proven useful in achieving wide-band disturbance rejection for various applications including, hard disk drives [Yi et al. (2009)], robotic manipulators [Yun and Su (2014)], and magnetic bearing [Rouhani et al. (2019a)] systems. Furthermore, several methods are used to design linear control systems for eliminating narrow-band disturbances. One of the most common approaches is introducing notch filters in the feedback control loop [Knospe et al. (1995)] and [Lei and Palazzolo (2008)]. However, this approach may perturb the feedback control loop too much which can result in instability. An alternative approach is to use the adaptive feedforward control (AFC) algorithm, which injects the proper sinusoidal signal to cancel narrow-band disturbances in a feedforward manner.

AFC algorithms based on the steepest gradient method have been popular for SISO systems [Ben Amara et al. (1999)] and [Shahsavari et al. (2017)], and the gradient AFC (GAFC) turns out to be approximately equivalent to a linear time invariant (LTI) system with an oscillator internal model [Guo and Bodson (2010)]. For SISO systems, the stability of GAFC has been proved using an averaging analysis for small adaptation gains [Bodson (1988)]. Also, in [Na and Park (1997)], the proposed GAFC maintains the stability of the original closed loop system. In contrast, for MIMO systems, the literature does not address the AFC and its applications extensively.

This paper reviews the GAFC design for MIMO discrete time linear systems, and it finds the approximate LTI equivalent form for the adaptive algorithm. Using the LTI equivalence for SISO systems, the GAFC with sufficiently small choice of adaptation gain is shown to be stable for any disturbance frequency. Motivated by the LTI analysis of the SISO GAFC, the inversion filter is introduced to convert the coupled MIMO system into the nearly decoupled SISO systems with fixed time delays using H-infinity synthesis. Then, the inversion based AFC (IAFC) is proposed by designing the GAFC for virtual SISO time delay systems. Finally, disturbance rejection for an open loop unstable and highly coupled MIMO Active Magnetic Bearing Spindle (AMBS) is investigated using both GAFC and the proposed IAFC methods.

2. PROBLEM SETUP AND ADAPTIVE ALGORITHM

2.1 Basic Idea and Features

The basic idea behind AFC can be illustrated in Figure 1, where $G(z)$ is a MIMO discrete time transfer function representing either an open-loop plant or a closed-loop plant consisting of an open-loop plant with a stabilizing feedback controller. The MIMO transfer function $G(z)$ is assumed to be square, $n \times n$, where n denotes its

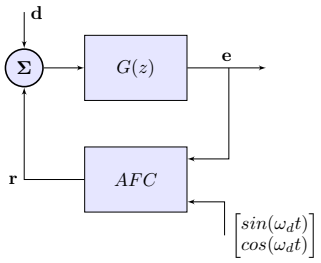

Fig. 1. Block diagram of the adaptive feedforward controller with sinusoidal regressors.

number of inputs and outputs. Furthermore, and *AFC* is the adaptive feedforward controller. The plant's and controller's outputs are $\mathbf{e}$ and $\mathbf{r}$ respectively, and $\mathbf{d}$ is assumed to be a sinusoidal disturbance as following:

$$\mathbf{d}(t) = \mathbf{c}sin(\omega_d t + \theta_d) \tag{1}$$

where $t(= 0, 1, 2, ...)$ is the sample time or sample number, $\omega_d = \omega_0 T_s$, ω_0 is the disturbance frequency, and T_s is the sampling time. Furthermore, $\mathbf{c}$ is the $n \times 1$ gain vector, and θ_d is the scalar phase. The goal of the controller is to minimize the plant output $\mathbf{e}$ by injecting the appropriate regressor signal $\mathbf{r}$.

2.2 Gradient AFC (GAFC)

To minimize the plant output $\mathbf{e}$, a gradient descent algorithm for the phase and gain of the reference signal $\mathbf{r}$ is used. The controller minimizes the following instantaneous cost:

$$\mathbf{J}(t) = \frac{1}{2}\mathbf{e}(t)^T\mathbf{e}(t) \tag{2}$$

where $\mathbf{J}$ is the cost, and T indicates the vector or matrix transpose. The AFC algorithm is based upon that the disturbance is at discrete frequencies. Therefore, $\mathbf{r}$ can be parameterized as:

$$\mathbf{r}(t) = \mathbf{a}(t)sin(\omega_d t) + \mathbf{b}(t)cos(\omega_d t) \tag{3}$$

where $\mathbf{a}$ and $\mathbf{b}$ are the $n \times 1$ unknown array of fourier coefficients, which the adaptive controller attempts to identify. The updates for the fourier coefficients are derived by a simple gradient descent law using the instantaneous cost in (2):

$$\begin{bmatrix}\mathbf{a}(t+1)\\ \\ \mathbf{b}(t+1)\end{bmatrix} = \begin{bmatrix}\mathbf{a}(t)\\ \\ \mathbf{b}(t)\end{bmatrix} - \mu \begin{bmatrix}\dfrac{\partial \mathbf{J}(t)}{\partial \mathbf{a}(t)}\\ \\ \dfrac{\partial \mathbf{J}(t)}{\partial \mathbf{b}(t)}\end{bmatrix} \tag{4}$$

where μ is the adaptation gain. Given that

$$\mathbf{e} = G(z)[\mathbf{d} + \mathbf{r}] \tag{5}$$

where the notation $G(z)[.]$ denotes the multivariable LTI transfer function $G(z)$ acting on the indicated vector discrete domain signal. Using the following chain rules,

$$\frac{\partial \mathbf{J}(t)}{\partial \mathbf{a}(t)} = \frac{\partial \mathbf{r}(t)}{\partial \mathbf{a}(t)}\frac{\partial \mathbf{e}(t)}{\partial \mathbf{r}(t)}\frac{\partial \mathbf{J}(t)}{\partial \mathbf{e}(t)} \tag{6}$$

$$\frac{\partial \mathbf{J}(t)}{\partial \mathbf{b}(t)} = \frac{\partial \mathbf{r}(t)}{\partial \mathbf{b}(t)}\frac{\partial \mathbf{e}(t)}{\partial \mathbf{r}(t)}\frac{\partial \mathbf{J}(t)}{\partial \mathbf{e}(t)} \tag{7}$$

gradients of the cost are:

$$\frac{\partial \mathbf{J}(t)}{\partial \mathbf{a}(t)} = (sin(\omega_d t)I_{n\times n})G^T(z)[\mathbf{e}(t)] \tag{8}$$

$$\frac{\partial \mathbf{J}(t)}{\partial \mathbf{b}(t)} = (cos(\omega_d t)I_{n\times n})G^T(z)[\mathbf{e}(t)] \tag{9}$$

where I is the identity matrix. Rearranging (8) and (9),

$$\frac{\partial \mathbf{J}(t)}{\partial \mathbf{a}(t)} = G^T(z)[sin(\omega_d t)I_{n\times n}]\mathbf{e}(t) \tag{10}$$

$$\frac{\partial \mathbf{J}(t)}{\partial \mathbf{b}(t)} = G^T(z)[cos(\omega_d t)I_{n\times n}]\mathbf{e}(t) \tag{11}$$

gradients can be shown as a product of filtered sinusoid at ω_0 and the plant output $\mathbf{e}$. The notation used here is that $G(z)[sin(\omega_d t)I_{n\times n}]$ is the transfer function acting on n columns of the indicated vector discrete domain signals. In the steady state, it can be shown:

$$\begin{bmatrix}G(z)[sin(\omega_d t)I_{n\times n}]\\ \\ G(z)[cos(\omega_d t)I_{n\times n}]\end{bmatrix} = \begin{bmatrix}G_R & G_I\\ \\ -G_I & G_R\end{bmatrix}\begin{bmatrix}sin(\omega_d t)I_{n\times n}\\ \\ cos(\omega_d t)I_{n\times n}\end{bmatrix} \tag{12}$$

where $G_R = Re[G(e^{j\omega_d})]$, $G_I = Im[G(e^{j\omega_d})]$, $j^2 = -1$ and $G(e^{j\omega_d}) = Re[G(e^{j\omega_d})] + jIm[G(e^{j\omega_d})]$. Using (12), gradients of the cost can be written as following.

$$\begin{bmatrix}\dfrac{\partial \mathbf{J}(t)}{\partial \mathbf{a}(t)}\\ \\ \dfrac{\partial \mathbf{J}(t)}{\partial \mathbf{b}(t)}\end{bmatrix} = \begin{bmatrix}G_R & -G_I\\ \\ G_I & G_R\end{bmatrix}^T\begin{bmatrix}sin(\omega_d t)I_{n\times n}\\ \\ cos(\omega_d t)I_{n\times n}\end{bmatrix}\mathbf{e}(t) \tag{13}$$

Then, the linear time variant (LTV) state-space representation of GAFC is shown as following:

$$\begin{bmatrix}\mathbf{a}(t+1)\\ \\ \mathbf{b}(t+1)\end{bmatrix} = \begin{bmatrix}I_{n\times n} & 0\\ \\ 0 & I_{n\times n}\end{bmatrix}\begin{bmatrix}\mathbf{a}(t)\\ \\ \mathbf{b}(t)\end{bmatrix} - \mu\begin{bmatrix}G_R & -G_I\\ \\ G_I & G_R\end{bmatrix}^T\begin{bmatrix}sin(\omega_d t)I_{n\times n}\\ \\ cos(\omega_d t)I_{n\times n}\end{bmatrix}\mathbf{e}(t) \tag{14}$$

$$\mathbf{r}(t) = [sin(\omega_d t)I_{n\times n}\ cos(\omega_d t)I_{n\times n}]\begin{bmatrix}\mathbf{a}(t)\\ \\ \mathbf{b}(t)\end{bmatrix} \tag{15}$$

2.3 LTI Equivalence of GAFC

The LTV state-space representation of GAFC in (14) and (15) can be transferred to new coordinates by the following non-singular linear transformation:

$$\begin{bmatrix}\mathbf{a}(t)\\ \mathbf{b}(t)\end{bmatrix} = M(t)\begin{bmatrix}\tilde{\mathbf{a}}(t)\\ \tilde{\mathbf{b}}(t)\end{bmatrix} \tag{16}$$

where,

$$M(t) = \begin{bmatrix} sin(\omega_d t)I_{n\times n} & -cos(\omega_d t)I_{n\times n} \\ cos(\omega_d t)I_{n\times n} & sin(\omega_d t)I_{n\times n}\end{bmatrix} \tag{17}$$

is a non-singular time variant matrix. The LTV state-space representation of GAFC has the following form in the new coordinate system.

$$\begin{bmatrix}\tilde{\mathbf{a}}(t+1)\\ \tilde{\mathbf{b}}(t+1)\end{bmatrix} = \begin{bmatrix} cos(\omega_d)I_{n\times n} & -sin(\omega_d)I_{n\times n} \\ sin(\omega_d)I_{n\times n} & cos(\omega_d)I_{n\times n}\end{bmatrix}\begin{bmatrix}\tilde{\mathbf{a}}(t)\\ \tilde{\mathbf{b}}(t)\end{bmatrix}$$
$$-\mu\begin{bmatrix} cos(\omega_d)G_R^T + sin(\omega_d)G_I^T \\ sin(\omega_d)G_R^T - cos(\omega_d)G_I^T\end{bmatrix}\mathbf{e}(t) \tag{18}$$

$$\mathbf{r}(t) = [I_{n\times n}\ 0\times I_{n\times n}]\begin{bmatrix}\tilde{\mathbf{a}}(t)\\ \tilde{\mathbf{b}}(t)\end{bmatrix} \tag{19}$$

(18) and (19) are the equivalent linear time invariant (LTI) state space representations of GAFC. Then, the multivariable LTI transfer function has the following form:

$$C_{GAFC}(z) = -\mu\frac{[G_R^T cos(\omega_d) + G_I^T sin(\omega_d)]z - G_R}{z^2 - 2cos(\omega_d)z + 1} \tag{20}$$

where $C_{GAFC}(z)$ is the GAFC LTI equivalent transfer function. The LTI equivalence facilitates stability and convergence analysis for the adaptive controller.

2.4 Stability and Convergence Rate

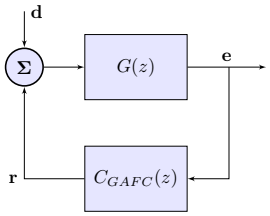

Fig. 2. Equivalent LTI feedback control system for the GAFC.

The most obvious usefulness of the LTI equivalence is to predict the stability of the adaptive controller for various adaption gains. Figure 2 shows the equivalent LTI feedback control system for GAFC. Transfer function from **d** to **e** is derived as following.

$$\mathbf{e} = G(z)[\mathbf{d} + \mathbf{r}] \tag{21}$$
$$\mathbf{r} = C_{GAFC}(z)[\mathbf{e}] \tag{22}$$
$$\mathbf{e} = G(z)[\mathbf{d}] + G(z)C_{GAFC}(z)[\mathbf{e}] \tag{23}$$
$$\mathbf{e} = (I_{n\times n} - G(z)C_{GAFC}(z))^{-1}G(z)[\mathbf{d}] \tag{24}$$

Therefore, the convergence and stability of GAFC for various adaptation gains can be checked by looking at the following number.

$$\mu_{conv} = 1 - max(abs[poles([I_{n\times n} - G(z)C_{GAFC}(z)]^{-1})]) \tag{25}$$

μ_{conv} is desired to be zero or a positive number for the stability, and closer to one for the fast convergence.

3. PROPOSED INVERSION BASED AFC (IAFC)

3.1 Motivation and Decoupling Technique

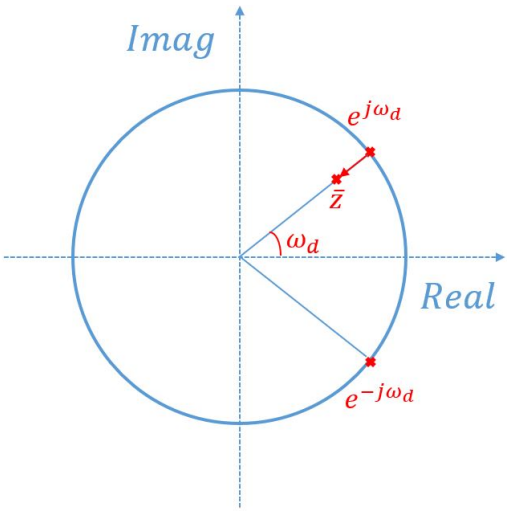

Fig. 3. Stability analysis for SISO GAFC.

It is known that the gradient algorithm is not stable for all adaptation gains, and its stability and convergence rate depend on the disturbance frequency. Using (25), the stability and convergence rate of the GAFC for SISO systems can be checked by looking at the following number.

$$\mu_{conv} = 1 - max(abs[poles(\frac{1}{1 - G(z)C_{GAFC}(z)})]) \tag{26}$$

Rewriting $G(e^{j\omega T_s})$ using the polar coordinate system,

$$G(e^{j\omega T_s}) = \psi(\omega)e^{j\phi(\omega)} \tag{27}$$

where $\psi(\omega)$ is the amplitude and $\phi(\omega)$ is the phase. Then, the LTI controller in (20) can be rearranged as following for SISO systems.

$$C_{GAFC}(z) = \frac{-\mu}{2}[\frac{\psi(\omega_0)e^{-j\phi(\omega_0)}e^{j\omega_d}}{z - e^{j\omega_d}} + \frac{\psi(\omega_0)e^{j\phi(\omega_0)}e^{-j\omega_d}}{z - e^{-j\omega_d}}] \tag{28}$$

In order to find the μ_{conv}, it is desired to study how the adaptation gain changes the roots of the following characteristic equation,

$$1 - G(z)C_{GAFC}(z) = 0 \tag{29}$$

which can be simplified to the following two equations.

$$\angle(G(z)C_{GAFC}(z)) = 0 \tag{30}$$
$$|G(z)C_{GAFC}(z)| = 1 \tag{31}$$

Here $\angle$ refers to the phase, and $||$ refers to the magnitude. Also, (30) can be more simplified as following:

$$\angle G(z) + \angle C_{GAFC}(z) = 0 \tag{32}$$

where

$$\angle C_{GAFC}(z) = \angle(e^{j(\omega_d - \phi(\omega_0))}(z - e^{-j\omega_d}) + e^{j(\phi(\omega_0)-\omega_d)}(z - e^{j\omega_d})) - \angle(z - e^{-j\omega_d}) - \angle(z - e^{j\omega_d}) + \pi \tag{33}$$

when $\mu \to 0$, μ_{conv} in (26) can be computed by finding the magnitude of the closest pole to $e^{j\omega_d}$, $\bar{z}$. Therefore by neglecting the term $\bar{z} - e^{j\omega_d}$, $\angle C_{GAFC}(\bar{z})$ is found to be the following.

$$\angle C_{GAFC}(\bar{z}) = \omega_d - \phi(\omega_0) + \frac{\pi}{2} - \angle(\bar{z} - e^{j\omega_d}) - \frac{\pi}{2} + \pi \tag{34}$$

Therefore, by assuming $\angle G(\bar{z}) = \phi(\omega_0)$, and combining (32) and (34), the following relationship exists.

$$\angle(\bar{z} - e^{j\omega_d}) = \omega_d - \pi \tag{35}$$

From (35), for the small value of μ, the departure angle is always pointing to the origin, and $\bar{z} - e^{j\omega_d}$ is on the radius of unit circle in the complex plane shown in Figure 3. This shows that a sufficiently small choice of the adaptation gain guarantees the GAFC stability.

Motivated by the stability of the SISO GAFC, a H-infinity model matching inversion filter is proposed to decouple the MIMO system into n Identical time delay SISO systems. In this method, decoupling is achieved by filtering the $\mathbf{e}$ signal through the inversion filter as following,

$$\mathbf{e_f} = F(z)[\mathbf{e}] \tag{36}$$

where $F(z)$ is the inversion filter. Combining (5) and (36),

$$\mathbf{e_f} = F(z)G(z)[\mathbf{r}] \tag{37}$$

and defining $G_f(z) = F(z)G(z)$, $G_f(z)$ is approximated to be a diagonal time delay transfer function by designing $F(z)$ such that the following cost is minimized.

$$J_\infty = \min_{F(z)\in RH_\infty} \left\| z^{-d} I_{n\times n} - F(z)G(z) \right\|_\infty \tag{38}$$

The optimization problem can be solved for the inversion filter $F(z)$ using standard γ iterations. The main tuning knob is the delay length d, which gives a better inversion as it is increased, but at the expense of robustness [Tsao (1994)]. By increasing d until J_∞ is small, the following approximation can be made

$$F(z)G(z) \approx z^{-d} I_{n\times n} \tag{39}$$

then

$$G_f(z) \approx z^{-d} I_{n\times n} \tag{40}$$

The idea behind proposed inversion based AFC (IAFC) is illustrated in Figure 4

3.2 Adaptive Algorithm

The goal of the proposed IAFC is to minimize the output of the inversion filter $\mathbf{e_f}$ at the specified disturbance

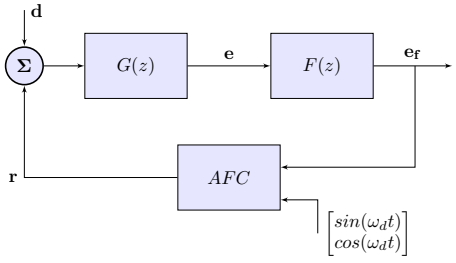

Fig. 4. Block diagram of the proposed IAFC with sinusoidal regressors.

frequency ω_0 by injecting the appropriate regressor signal $\mathbf{r}$. To minimize $\mathbf{e_f}$ a gradient descent algorithm is used to find the fourier coefficients of $\mathbf{r}$. The proposed controller minimizes the following instantaneous cost.

$$\mathbf{J}(t) = \frac{1}{2}\mathbf{e_f}(t)^T \mathbf{e_f}(t) \tag{41}$$

Since $z^{-d} = e^{-jw_d d} = cos(w_d d) - jsin(w_d d)$, and using (13) and (40), gradients of the cost for IAFC can be obtained as following:

$$\begin{bmatrix} \frac{\partial \mathbf{J}(t)}{\partial \mathbf{a}(t)} \\ \\ \frac{\partial \mathbf{J}(t)}{\partial \mathbf{b}(t)} \end{bmatrix} = \begin{bmatrix} cos(\omega_d d) I_{n\times n} & sin(\omega_d d) I_{n\times n} \\ \\ -sin(\omega_d d) I_{n\times n} & cos(\omega_d d) I_{n\times n} \end{bmatrix} \times \begin{bmatrix} sin(\omega_d t) I_{n\times n} \\ \\ cos(\omega_d t) I_{n\times n} \end{bmatrix} \mathbf{e_f}(t) \tag{42}$$

which can finally be simplified to:

$$\begin{bmatrix} \frac{\partial \mathbf{J}(t)}{\partial \mathbf{a}(t)} \\ \\ \frac{\partial \mathbf{J}(t)}{\partial \mathbf{b}(t)} \end{bmatrix} = \begin{bmatrix} sin(\omega_d(t+d)) I_{n\times n} \\ \\ cos(\omega_d(t+d)) I_{n\times n} \end{bmatrix} \mathbf{e_f}(t) \tag{43}$$

3.3 LTI Equivalence of Inversion Based AFC

Using (4) and (43), the LTV state-space representation of the IAFC is shown as following.

$$\begin{bmatrix} \mathbf{a}(t+1) \\ \\ \mathbf{b}(t+1) \end{bmatrix} = \begin{bmatrix} I_{n\times n} & 0 \\ \\ 0 & I_{n\times n} \end{bmatrix} \begin{bmatrix} \mathbf{a}(t) \\ \\ \mathbf{b}(t) \end{bmatrix} - \mu \begin{bmatrix} sin(\omega_d(t+d)) I_{n\times n} \\ \\ cos(\omega_d(t+d)) I_{n\times n} \end{bmatrix} \mathbf{e_f}(t) \tag{44}$$

$$\mathbf{r}(t) = [sin(\omega_d t) I_{n\times n} \; cos(\omega_d t) I_{n\times n}] \begin{bmatrix} \mathbf{a}(t) \\ \\ \mathbf{b}(t) \end{bmatrix} \tag{45}$$

Applying the state transformation described in (16) and (17), the LTI equivalence of the IAFC has the following state space representation:

$$\begin{bmatrix}\tilde{\mathbf{a}}(t+1)\\ \tilde{\mathbf{b}}(t+1)\end{bmatrix} = \begin{bmatrix}cos(\omega_d)I_{n\times n} & -sin(\omega_d)I_{n\times n}\\ sin(\omega_d)I_{n\times n} & cos(\omega_d)I_{n\times n}\end{bmatrix}\begin{bmatrix}\tilde{\mathbf{a}}(t)\\ \tilde{\mathbf{b}}(t)\end{bmatrix} - \mu\begin{bmatrix}cos(\omega_d(1+d))I_{n\times n}\\ sin(\omega_d(1+d))I_{n\times n}\end{bmatrix}\mathbf{e_f}(t) \tag{46}$$

$$\mathbf{r}(t) = [I_{n\times n}\ 0\times I_{n\times n}]\begin{bmatrix}\tilde{\mathbf{a}}(t)\\ \tilde{\mathbf{b}}(t)\end{bmatrix} \tag{47}$$

which can be used to find the equivalent LTI transfer function.

$$C_{IAFC}(z) = -\mu\frac{cos(\omega_d(1+d))z - cos(\omega_d)}{z^2 - 2cos(\omega_d)z + 1}I_{n\times n} \tag{48}$$

3.4 Stability and Convergence Rate

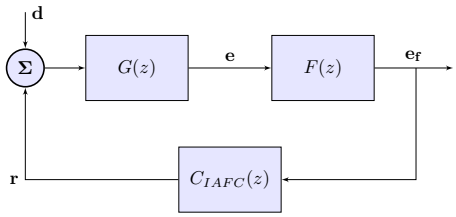

Fig. 5. Equivalent LTI feedback control system for the IAFC.

Figure 5 shows the equivalent LTI feedback control system for the IAFC, where $C_{IAFC}(z)$ is the LTI equivalent controller. Transfer function from $\mathbf{d}$ to $\mathbf{e}$ is derived as following.

$$\mathbf{e} = G(z)[\mathbf{d}+\mathbf{r}] \tag{49}$$
$$\mathbf{e_f} = F(z)[\mathbf{e}] \tag{50}$$
$$\mathbf{r} = C_{IAFC}(z)[\mathbf{e_f}] \tag{51}$$
$$\mathbf{e} = G(z)[\mathbf{d}] + G(z)C_{IAFC}(z)F(z)[\mathbf{e}] \tag{52}$$
$$\mathbf{e} = (I_{n\times n} - G(z)C_{IAFC}(z)F(z))^{-1}G(z)[\mathbf{d}] \tag{53}$$

Therefore, the convergence and stability of IAFC for various adaptation gains can be checked by looking at the following number.

$$\mu_{conv} = 1 - max(abs[poles([I_{n\times n} - G(z)C_{IAFC}(z)F(z)]^{-1})]) \tag{54}$$

4. MAGNETIC BEARING APPLICATION

4.1 System Description and Experimental Setup

The application of the AFC is well suited for an open-loop unstable MIMO (4×4) Active Magnetic Bearing Spindle (AMBS) shown in Figure 6. The experimental system is explained in details in [Rouhani et al. (2019b)], and a Linear-Quadratic-Gaussian with Integral action discussed in [Rai et al. (2016)is used as the baseline controller to stabilize the plant and levitate the rotor. Figure 7 shows the block diagram of the proposed IAFC for the AMBS, where $C(z)$ and $P(z)$ represent the two degrees of freedom (2-dof) LQGi controller and the plant respectively. Furthermore, $\mathbf{u}$, $\mathbf{u_f}$ and $\mathbf{y}$ are the control input, the filtered input and the measurement output respectively. The IAFC here is proposed to allow the rotor to spin at 500 Hz, which can be modeled as the disturbance frequency, about its inertial axis with minimal control effort, $\mathbf{u}$.

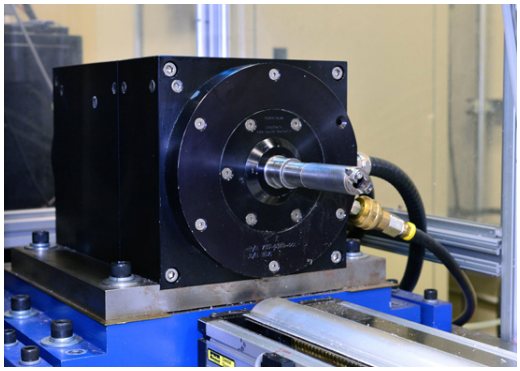

Fig. 6. Picture of AMBS system.

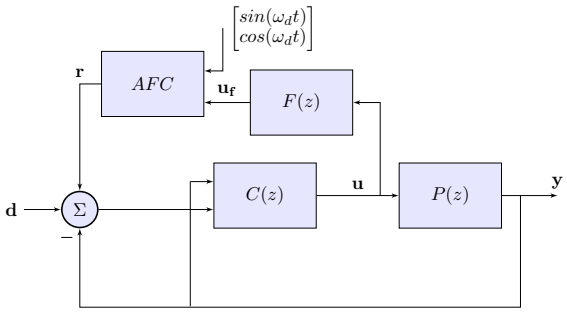

Fig. 7. Block diagram of the proposed IAFC for the AMBS.

4.2 LTI Analysis and Simulation Results

The proposed IAFC is designed to minimize the control effort $\mathbf{u}$ while rejecting the 500 Hz sinusoidal disturbance. Therefore, the appropriate closed-loop transfer function in the adaptive algorithm $G(z)$ is obtained by finding the transfer function from $\mathbf{d}$ to $\mathbf{u}$. Since the baseline controller is 2-dof, it can be decomposed as,

$$C(z) = [C_1(z)\ C_2(z)] \tag{55}$$

where $C_1(z)$ corresponds to the y and $C_2(z)$ corresponds to the $\mathbf{d}-\mathbf{y}$. Then $G(z)$ have the following form:

$$G(z) = [I_{4\times 4} - (C_1(z) - C_2(z))P_n(z)]^{-1}C_2(z) \tag{56}$$

where $P_n(z)$ is a 20th order nominal plant model obtained in [Rai et al. (2016)]. The inversion filter, $F(z)$, is obtained by solving the model matching problem in (38) with the delay length 10. By LTI stability analysis, Figure 8 shows that the proposed IAFC converges more than 100 faster for various adaptation gains in comparison with the GAFC. Simulation results in Figure 9 also verifies the significant faster convergence rate of the proposed IAFC.

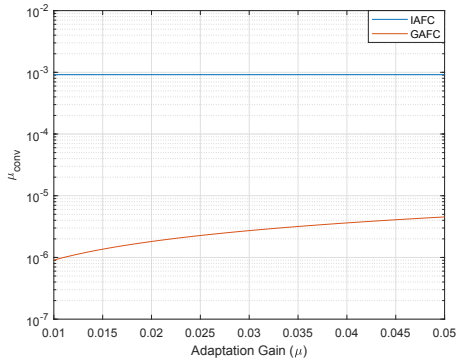

Fig. 8. Convergence rates VS adaptation gains at 500 Hz.

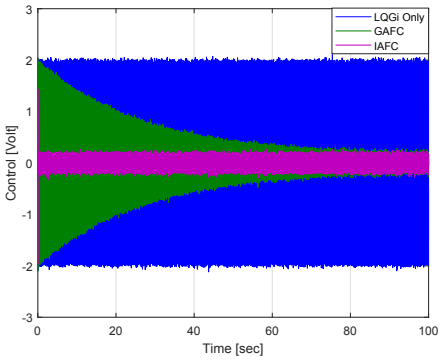

Fig. 9. The control signal for one input channel with the sinusoidal disturbance at 500 Hz.

In simulation, a normally distributed random signal is added to the output to show the possible measurement noises. The noise is zero mean and 0.05 standard deviation. Furthermore, a 100th order model is used as a plant model to simulate the algorithm in a more realistic scenario while the 20th order model is used for LQGi, GAFC and IAFC design.

4.3 Experimental Results

In the experiment, spindle is kept spinning at 500 Hz and then steady-state data is collected. Since GAFC has a slow convergence rate, only the IAFC is implemented in the experiment. Figure 10 shows adding IAFC reduces the control effort by 100 dB at the spin frequency in comparison with operating only with the baseline controller.

5. CONCLUSION

In this paper, a novel AFC design is developed for MIMO discrete time linear systems. The stability of the proposed IAFC is proven using the LTI analysis, and its performance is evaluated on a MIMO unstable AMBS system. Simulation and experimental results show the effectiveness of the proposed IAFC.

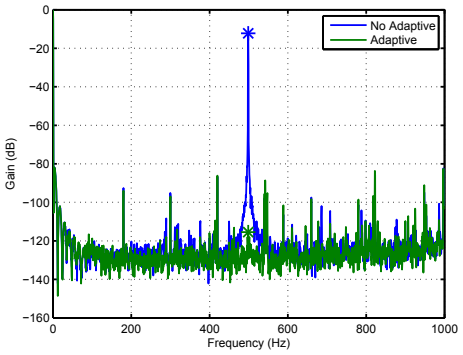

Fig. 10. Power Spectral Density of the control signal for one input channel with the spindle spinning at 500 Hz.

REFERENCES

Ben Amara, F., Kabamba, P.T., and Ulsoy, A.G. (1999). Adaptive sinusoidal disturbance rejection in linear discrete-time systems—part i: Theory. *Journal of Dynamic Systems, Measurement, and Control*, 121(4), 648–654.

Bodson, M. (1988). Effect of the choice of error equation on the robustness properties of adaptive control systems. *International Journal of Adaptive Control and Signal Processing*, 2(4), 249–257.

Guo, X. and Bodson, M. (2010). Equivalence between adaptive feedforward cancellation and disturbance rejection using the internal model principle. *International journal of adaptive control and signal processing*, 24(3), 211–218.

Knospe, C.R., Hope, R.W., Fedigan, S.J., and Williams, R.D. (1995). Experiments in the control of unbalance response using magnetic bearings. *Mechatronics*, 5(4), 385–400.

Lei, S. and Palazzolo, A. (2008). Control of flexible rotor systems with active magnetic bearings. *Journal of Sound and Vibration*, 314(1-2), 19–38.

Na, H.S. and Park, Y. (1997). An adaptive feedforward controller for rejection of periodic disturbances. *Journal of Sound and Vibration*, 201(4), 427–435.

Rai, S., Cavalier, G., Simonelli, J., and Tsao, T.C. (2016). Mimo repetitive control of an active magnetic bearing spindle. *IFAC-PapersOnLine*, 49(21), 192–199.

Rouhani, S., Tsao, T.C., and Speyer, J.L. (2019a). Multivariable disturbance observer based control with the experiment on an active magnetic bearing spindle. *IFAC-PapersOnLine*, 52(15), 388–393.

Rouhani, S., Tsao, T.C., and Speyer, J.L. (2019b). Robust disturbance estimation-an integrated game theoretic and unknown input observer approach. In *2019 American Control Conference (ACC)*, 5077–5082. IEEE.

Shahsavari, B., Pan, J., and Horowitz, R. (2017). An adaptive feedforward control approach for rejecting disturbances acting on uncertain linear systems. In *ASME 2016 Dynamic Systems and Control Conference*. American Society of Mechanical Engineers Digital Collection.

Tsao, T.C. (1994). Optimal feed-forward digital tracking controller design. *Journal of dynamic systems, measurement, and control*, 116(4), 583–592.

Yi, J., Chang, S., and Shen, Y. (2009). Disturbance-observer-based hysteresis compensation for piezoelectric actuators. *IEEE/Asme transactions on mechatronics*, 14(4), 456–464.

Yun, J.N. and Su, J.B. (2014). Design of a disturbance observer for a two-link manipulator with flexible joints. *IEEE Transactions on Control Systems Technology*, 22(2), 809–815.